Acta Oceanol. Sin., 2025, Vol. 44, No. 4, P. 20–34
https://doi.org/10.1007/s13131-025-2462-8

Redox condition changes in the Ross Sea, Antarctica, since the last glacial maximum

Yizhuo Wang[1, 2, 3], Yi Zhang[2, 3], Xibin Han[2, 3*], Li Lin[1], Yukai Hong[2, 3], Rui Han[2, 3, 4], Yun Liu[2, 3, 4], Pengyun Ma[2, 3, 4], Qian Ge[2, 3], Xiaohu Li[2, 3]

[1] Institute of Sedimentary Geology, Chengdu University of Technology, Chengdu 610059, China
[2] Second Institute of Oceanography, Ministry of Natural Resources, Hangzhou 310012, China
[3] State Key Laboratory of Submarine Geoscience, Hangzhou 310012, China
[4] College of Geodesy and Geomatics, Shandong University of Science and Technology, Qingdao 266590, China

Received 15 October 2024; accepted 28 February 2025
© Chinese Society for Oceanography and Springer-Verlag GmbH Germany, part of Springer Nature 2025

Abstract

Research on changes in the redox conditions of bottom waters is essential for understanding deep water circulation, global ocean currents, climate change, and ecosystem health. Through sedimentary geological methods, a deeper understanding of the complex relationships between various environmental changes can be achieved, providing detailed evidence and theoretical support for global climate change research. The Ross Sea in Antarctica plays a key role in the formation of Antarctic bottom water (AABW), and the complex climate changes since the last glacial maximum (LGM) make it particularly significant for study. This research analyzes core ANT32-RB16C from the Ross Sea using geochemical proxies such as major and trace elements, grain size, and redox-sensitive indicators like Mn/Ti, Co/Ti, Mo/Ti, Cd/Ti, U/Th, and Ni/Co molar concentration ratios. Combining this data with a previously established chronological framework, the study explores the evolution of redox conditions in the Ross Sea's deep waters since the LGM. The results show that the deep waters have remained oxygen-rich since the LGM, with significant changes in four stages. Stage 1 (24.7–15.7 cal ka BP): Strong oxidizing conditions, likely due to enhanced formation of Ross Sea bottom water (RSBW), increasing oxygen levels. Stage 2 (15.7–4.5 cal ka BP): Weakened oxidizing conditions as temperatures rose and ice shelves retreated, increasing primary productivity and depleting oxygen. Stage 3 (4.5–1.5 cal ka BP): Continued decline in oxidizing conditions, possibly linked to high primary productivity and oxygen consumption. Stage 4 (1.5 cal ka BP to present): A rapid recovery of oxidizing conditions, likely driven by temperature drops, increased RSBW formation, and decreased productivity.

Key words redox environment, Ross Sea, last glacial maximum, bottom waters, geochemical redox-sensitive element proxies

Citation Wang Yizhuo, Zhang Yi, Han Xibin, Lin Li, Hong Yukai, Han Rui, Liu Yun, Ma Pengyun, Ge Qian, Li Xiaohu. 2025. Redox condition changes in the Ross Sea, Antarctica, since the last glacial maximum. Acta Oceanologica Sinica, 44(4): 20–34, doi: 10.1007/s13131-025-2462-8

1 Introduction

In modern oceans, the redox conditions of bottom waters are commonly classified into four categories (oxic, suboxic, anoxic, and euxinic) based on dissolved oxygen levels and hydrogen sulfide concentrations (Tribovillard et al., 2006). The redox environments are primarily influenced by the supply and consumption of oxygen (Colman and Holland, 2000; Ozaki and Tajika, 2013). It is generally believed that two main factors affect oxygen levels in water (Rabalais et al., 2002). Oxygen enters deep waters through ocean circulation, creating oxic environments when deep water formation is strong. Conversely, intensified water stratification or weakened circulation reduces the supply of oxygen, leading to hypoxic or euxinic conditions (Lenton, 2000; Ozaki and Tajika, 2013). Second, the

Foundation item: The National Key R&D Program of China under contract No. 2023YFC28 11305; the Scientific Research Fund of the Second Institute of Oceanography, MNR under contract No. SZ2405; the Impact and Response of Antarctic Seas to Climate Change under contract No. IRASCC.
*Corresponding author, E-mail: hanxibin@sio.org.cn

deposition of organic matter, driven by increased primary productivity, can significantly impact oxygen levels, thereby altering redox conditions (Algeo et al., 2010; Meyer et al., 2016; Ozaki and Tajika, 2013). Additionally, changes in ice shelf and sea ice coverage regulate gas exchange and water mixing, affecting oxygen transport (Baloza et al., 2022, 2023; Huang et al., 2023). Huang et al. (2023) reconstructed the retreat history of the Ross Ice Shelf since the LGM using core ANT31-JB06, highlighting its role in regulating deep-water oxygenation. Global ocean circulation, particularly the Atlantic meridional overturning circulation (AMOC) and Ross Sea bottom water (RSBW), also influences oxygen levels through changes in deep water ventilation intensity (Guo et al., 2016; Zhang et al., 2019).

As the hub of global ocean circulation, the Southern Ocean plays a crucial role in climate regulation and marine systems. Within this framework, RSBW plays an essential role. It not only drives deep water circulation and ventilates the deep ocean but also supplies oxygen-rich water to the global oceans, influencing redox conditions worldwide (Jacobs et al., 1970; Orsi and Wiederwohl, 2009). The Ross Sea, the second largest marginal sea of the Southern Ocean, is a significant source of Antarctic bottom water (AABW). Approximately 20% of AABW is derived from RSBW (Carmack and Killworth, 1978; Rintoul, 1985), making it a key factor in regional material cycling (Xiu et al., 2020). The northward expansion and southward retreat of RSBW affect deep circulation in the Southern Ocean, which in turn influences sensitive global climate shifts (Olund et al., 2018; Xiu et al., 2020). Therefore, changes in the redox conditions of the Ross Sea are of particular significance, as they exert a direct influence on the redox state of the global ocean.

Research on the redox environment in the Ross Sea has predominantly focused on the effects of climate change, sea ice coverage, bottom water circulation, and biological productivity. Climate change has a significant effect on redox environments, particularly through temperature and sea ice fluctuations. During glacial periods, low temperatures and extensive sea ice coverage hinder oxygen replenishment to deep waters, creating hypoxic, reducing conditions (Kajanto et al., 2024). However, with the onset of interglacial periods, reduced sea ice cover and enhanced bottom water upwelling improve oxygen supply to deep waters, improving the oxidative environment (Matthews and Briffa, 2005). Nevertheless, in some cases, even during warmer periods, the oxygen supply to deep waters remains insufficient, resulting in low oxygen conditions in some areas.

Changes in biological productivity are another important factor affecting redox conditions. Increased productivity leads to greater organic matter deposition and decomposition, which in turn consumes more oxygen. Research has shown that while primary productivity increased in certain periods of the Ross Sea, this also resulted in increased organic carbon decomposition, further depleting oxygen and reducing the oxidation environment (Kajanto et al., 2024). Additionally, the changes in the molar concentration ratios of Mn/Ti, Mo/Ti, and Cd/Ti can reflect shifts in redox conditions. For instance, increases in Mn/Ti ratios are associated with enhanced oxidative conditions, while Mo/Ti ratios are linked to the intensification of reducing environments (Matthews Briffa, 2005). The Cd/Ti ratio, on the other hand, may be related to the formation of sulfur compounds, particularly in periods of complex redox shifts, where the binding and desorption of cadmium and sulfur directly influence concentrations (Landais et al., 2015). These factors together help explain the dynamic changes in the redox environment of the Ross Sea.

Previous studies have shown that the deep waters of the Ross Sea have remained oxic since the LGM, with four notable oxic pulses. These pulses are linked to enhanced RSBW formation and low surface water productivity in the Ross Sea, while the termination of these oxic events likely contributed to rapid increases in atmospheric pCO_2 (Wang et al., 2018). However, Song et al. (2019) suggested that the redox conditions in the Ross Sea since the LGM are less influenced by RSBW and organic matter, and more shaped by ice shelf and sea ice dynamics. To study the redox conditions of deep oceans, multiple proxies such as petrology, paleontology, elemental geochemistry, and isotopic geochemistry have been developed (Mansour et al., 2020; Fan et al., 2020). While each proxy has its advantages in specific geological settings, the redox conditions they reflected can vary across different sedimentary environments (Fan et al., 2022). Among them, redox-sensitive element (RSE) are widely used due to their highly responsive behavior in varying sedimentary settings and broad applicability (Russell and Morford, 2001). Using a combination of multiple elemental proxies allows for more accurate reconstructions of redox conditions in deep waters (Tribovillard et al., 2006; Wang et al., 2018), which is a distinct advantage of RSE over other proxies.

Therefore, this study analyzes core ANT32-RB16C from the Ross Sea, examining major and trace elements, grain size, organic carbon, and nitrogen isotopes. Appropriate redox proxies were selected, and together with the chronological framework of the core, the study explores the changes in redox conditions in the Ross Sea since the LGM and their influencing factors. This study aims to provide novel insights into the redox conditions of the Ross Sea by integrating multiple redox proxies, thereby advancing our understanding of the intricate relationships between global ocean circulation and climate change. At the same time, this research fills some gaps in the study of redox environments in the region and provides detailed evidence and theoretical support for research on global climate change.

2 Regional overview

The Ross Sea, located in the Pacific sector of the Southern Ocean south of 70°S, is bordered by Victoria Land to the west and King Edward Ⅶ Land to the east, with the Transantarctic Mountains to the west and the Ross Ice Shelf (RIS) to the south (Anderson et al., 2014; Mosola and Anderson, 2006; Smith et al., 2012). It forms a near-triangular marine region (Fig. 1). The southern part of the Ross Ice Shelf is the largest ice shelf in the world, covering approximately 45 000 km². The central and eastern portions are primarily fed by the West Antarctic ice sheet (WAIS), while the western section is mainly supplied by the East Antarctic ice sheet (EAIS) (Anderson et al., 2002).

The sea ice in the Ross Sea exhibits clear seasonal variability. In winter, sea ice can expand as far north as 59°S; during the summer, the coverage reduces to about 20% of its winter extent, with ice remaining only in the eastern shelf edge and along certain coastal regions of Victoria Land (Liu et al., 2016). During the LGM, both the coverage and thickness of the sea ice increased, extending northward to the outer continental shelf (Muratli et al., 2010). Although most of the ice shelf is grounded on the continental shelf, some bottom domes formed at the leading edge of the ice shelf (Anderson et al., 2014; Smith et al., 2014). According to Licht et al. (1999), the grounding line of the ice shelf did not extend beyond 74°S in the western Ross Sea during the LGM. As deglaciation progressed, the RIS began to retreat significantly, although the extent of this retreat varied due to different climatic events. This retreat persisted into the early Holocene (11.7–9.0 ka), with the process largely halting by around 5 ka due to the influence of subglacial lakes (Huang et al., 2005).

Key water masses in the Ross Sea include Antarctic surface water (AASW), RSBW, circumpolar deep water (CDW), modified circumpolar deep water (MCDW), dense shelf water (DSW), and ice shelf water (ISW) (Fig. 1). Near the Antarctic continent, AASW circulates counterclockwise, with summer temperatures reaching up to 2.0℃ and salinities ranging from 33.5 to 34.5. RBSW can transport meltwater from the eastern Amundsen Sea into the Ross Sea (Smith et al., 2014). DSW, characterized by low temperatures, high salinity, and high density, forms during sea ice production (Basak et al., 2015). The formation of DSW is influenced by the advance and retreat of the RIS (Tamura et al., 2008). CDW is the most widespread water mass in the Southern Ocean and mixes with other water masses in the Ross Sea to transform into the warmer, less saline MCDW that flows onto the continental shelf (Dinniman et al., 2011; Yokoyama et al., 2016). Due to its relatively warm temperature, MCDW significantly influences the ice shelves and biological productivity.

Modern sea ice in the Ross Sea is predominantly composed of annual ice, with multi-year ice found only along the coast of Victoria Land and the western continental slope (Smith et al., 2014). The distribution of modern ice shelves shows notable seasonal changes; during the Southern Hemisphere's winter, the maximum extent is typically reached in September, covering nearly the entire

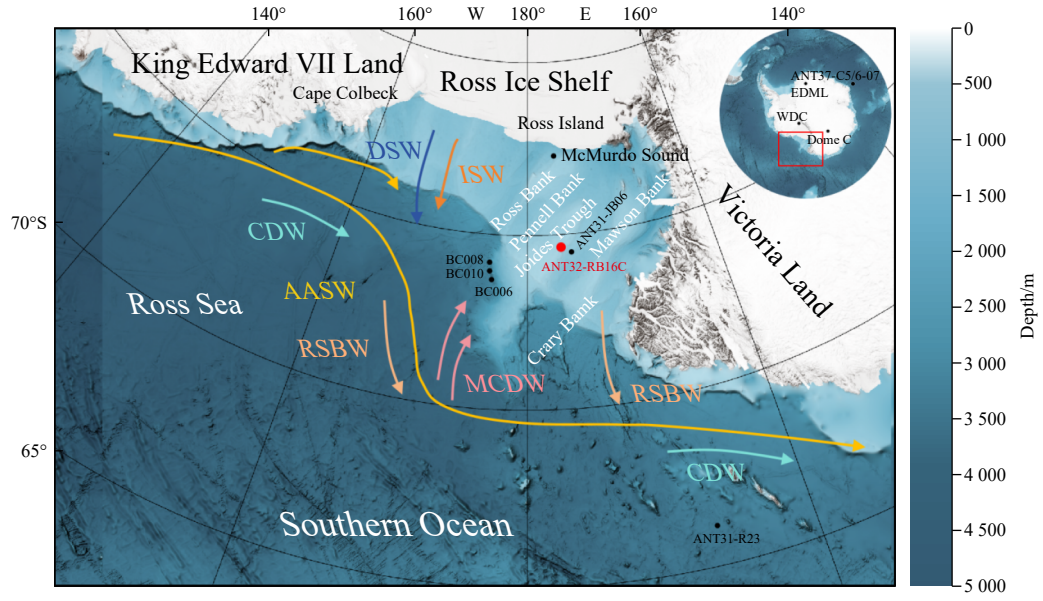


Fig. 1. Location of ANT32-RB16C and other sediment cores, along with circulation patterns in the Ross Sea. The positions of ANT32-RB16C, ANT31-R23 (Wang et al., 2018), ANT31-JB06 (Huang et al., 2016), ANT37-C5/6-07 (Hu et al., 2023), EDML (Fischer et al., 2007), WDC (WAIS Divide Project Members, 2015), Dome C (Monnin et al., 2004; Schmitt et al., 2012), and BC006, BC008, BC010 (Cui et al., 2021) were marked. AASW: Antarctic surface water; RSBW: Ross Sea bottom water; DSW: dense shelf water; CDW: circumpolar deep water; MCDW: modified circumpolar deep water; ISW: ice shelf water.

Ross Sea continental shelf. In summer, the sea ice coverage decreases dramatically, reaching its minimum in February (Gersonde et al., 2005; Stammerjohn et al., 2012). The unique topography of the Ross Sea promotes the formation of katabatic winds, which reduce ice concentrations along the front of the RIS and the coast of Victoria Land. This reduction in ice coverage allows polynyas and open water areas to form during the summer months (Pease, 1987). These polynyas contribute to the production of sea ice and serve as a significant source of high-salinity shelf water.

3 Samples and methods

3.1 *Samples*

The study focuses on the ANT32-RB16C sediment core collected from the northwest continental shelf of the Ross Sea by China's 32nd Antarctic Scientific Expedition (74°31′06″S, 175°07′15″E, water depth 471 m). The total length of the sediment core sample is 232 cm, and its lithology is uniform, consisting primarily of sandy silt. Based on the stratigraphic characteristics of the sediment core, it can be roughly divided into four segments from top to bottom.

(1) 0–6 cm

Yellow-green, soft texture, weakly cohesive, no distinct order, well-sorted, composed of gray-green diatomaceous clayey silt.

(2) 6–74 cm

Yellow-green, soft texture, weakly cohesive, no distinct order, well-sorted, containing sandy clay with hard cores, comprising gray-green silty clay.

(3) 74–161 cm

Dark gray, soft texture, weakly cohesive, no distinct order, contains gravel, primarily clay with silt, comprising dark gray clayey silt with grains.

(4) 161–232 cm

Dark gray, denser texture, weakly cohesive, no distinct order, reduced gravel content, containing sandy gravel and hard cores, primarily clay with silt, comprising dark gray clayey silt.

3.2 *Redox condition proxies*

To exclude the effects of diagenesis (Ordoñez et al., 2024), a significant concentration of RSE in the water can serve as an indicator of oxygen levels at the bottom waters and the water-rock interface (Brown et al., 2000; Calvert and Pedersen, 1993). Different RSEs have varying sensitivities to the redox conditions of the water, leading to their accumulation in sediments under different redox environments (Tribovillard et al., 2006).

Manganese (Mn) tends to form manganese oxides [Mn (Ⅳ)] under oxidizing conditions, while in reducing or suboxic conditions, it dissolves in the form of ionic manganese [Mn (Ⅱ)] (Calvert and Pedersen, 1993, 1996). Thus, the concentration of Mn in sediment records can reflect ancient redox changes. Cobalt (Co) is similarly controlled by redox conditions, and in marine sediments, it readily adsorbs onto Fe-Mn oxides, co-precipitating with them under oxidizing conditions. Therefore, both Mn and Co can serve as indicators of oxidation intensity. Molybdenum (Mo) and cadmium (Cd) present different variations compared to Mn and Co in different redox environments. For example, in oxygen-rich to suboxic waters, Mo and Cd exist in stable ionic forms, while Mn and Co precipitate from the water. In anoxic waters, the situation is reversed. Due to its strong affinity for sulfur, Mo readily forms sulfide solid solutions when a certain amount of H_2S is present in the water, strongly adsorbing Mo and reacting to produce $MoO_{4-X}S_X^{2-}$, which adsorbs onto humic/organic matter surfaces, forming authigenic precipitates (Adelson et al., 2001; Calvert and Pedersen, 1993, 1996; Xu et al., 2007). Similarly, Cd responds to redox conditions much like Mo. In reducing environments, Cd reacts with sulfide (S^{2-}) to form insoluble CdS, leading to its enrichment in sediments. Under oxic conditions, Cd remains dissolved as Cd^{2+}, but in suboxic to sulfidic environments, sulfate reduction produces H_2S, releasing S^{2-}. Cd^{2+} then precipitates as CdS, which is highly stable in anoxic conditions and resistant to reoxidation. Thus, Mo and Cd can serve as an indicator of reducing environments. Titanium (Ti) is a common terrigenous element, and due to its chemical stability, it is less affected by changes in seawater redox conditions. It can be used as a correction factor for the dilution effects of other elements, thereby excluding the influence of terrigenous components on sediments.

The ratios of Ni/Co and U/Th are commonly used to reflect the redox conditions of water. Both elements tend to accumulate under suboxic or anoxic conditions, but their accumulation in sediments varies due to their differing geochemical properties. Therefore, their ratios can indicate the reducing state of the water (Chang et al., 2009). The Ni/Co and U/Th ratios are particularly suitable for quantitative analysis due to their regularity and sensitivity to redox conditions (Tribovillard et al., 2006; Algeo and Maynard, 2004). The elements in these ratios exhibit significant distribution differences under varying redox conditions, and their geochemical behavior is stable, primarily controlled by redox conditions. This allows these ratios to provide a reliable and quantitative evaluation of redox condition (Morford and Emerson, 1999). Furthermore, they have been widely validated in numerous studies, making them a robust tool for assessing redox environments (Wignall and Twitchett, 1996; Algeo and Liu, 2020; Wei, 2012). The corresponding relationships are summarized in Table 1.

Therefore, this study ultimately uses the Ti-normalized element ratios of Mn/Ti and Co/Ti as proxies for the oxidation intensity in the study area, while Mo/Ti, Cd/Ti, U/Th, and Ni/Co serve as proxies for the redox environment. Additionally, U/Th and Ni/Co are selected as quan-

Table 1. Geochemical indicators of redox-sensitive elements (Tribovillard et al., 2006)

	U/Th	Ni/Co
Oxic	<0.75	<5
Suboxic	0.75–1.25	5–7
Anoxic	>1.25	>7

titative indicators for describing the redox conditions, allowing for a comprehensive investigation of changes in the redox environment.

3.3 *Grain size*

The advance and retreat of sea ice have significant effects on redox conditions. In addition to the $ssNa^+$ (sea-salt sodium) content in ice cores, sediment grain size fractions greater than 63 μm can be considered ice-rafted debris (IRD) (Diekmann and Kuhn, 1999; Lei et al., 2022; Li et al., 2015). Changes in IRD reflect historical climate changes and glacial activities. Analyzing IRD in sediments allows for the reconstruction of ancient depositional environments and reveals the processes of glacial expansion and retreat, which can provide insights into redox conditions (Liu et al., 2015). In this study, the grain size fraction greater than 63 μm from the ANT32-RB16C core is selected as a proxy for ice-rafted debris.

4 Results

4.1 *Age framework*

The method used to establish the age model for the sediment was based on the research findings of Song Lehui (Song et al., 2019). Radiometric dating was performed using ^{210}Pb and total carbon samples from the sediment, resulting in an age of 5 008 a BP for the top of the core and 29 712 a BP for the bottom (Fig. 2).

Combining previous studies (Anderson et al., 2002), the results from ^{210}Pb and total carbon dating were calculated, with the result of 5 008 a BP being designated as the old carbon age. After accounting for the influence of old carbon age at each depth level, the final calendar ages were determined: the top of the sediment core is 0 a BP, and the bottom age is 24 762 a BP (Table 2). This timeframe corresponds to the early stage of LGM (Song et al., 2019).

4.2 *Variations in redox proxies*

To eliminate the influence of different elemental concentration magnitudes and ensure comparability in statistical analysis, this study applied *Z*-score standardization to redox-sensitive elements and other indicators during result analysis (Jolliffe, 2002). The *Z*-score standardized re-

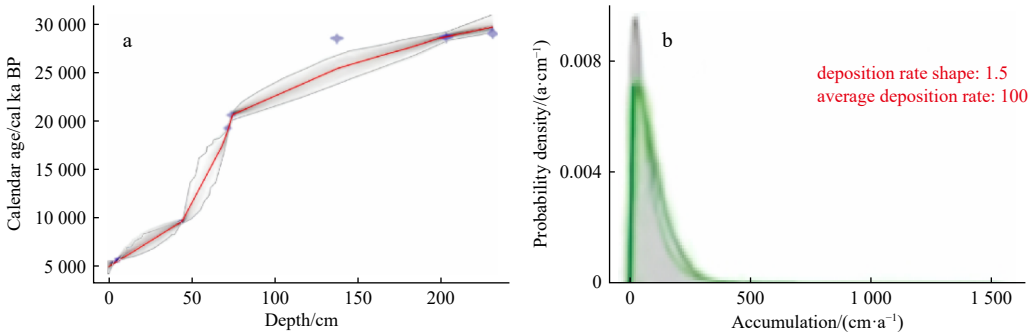


Fig. 2. Depositional rates of sample ANT32-RB16C (a), probability density and differentiation patterns of sample ANT32-RB16C (b).

Table 2. AMS^{14}C data and calendar age of core ANT32-RB16C

Sedimentary layer/cm	Sample material	Observed value/a	(Reservoir age + Old carbon age)/a	Calibrated age/a BP
0–2	Organic carbon	6 000 ± 30	5 008	0
4–6	Organic carbon	5 150 ± 30	5 008	521
6–8	Organic carbon	5 440 ± 30	5 008	778
42–44	Organic carbon	9 620 ± 40	5 008	–
44–46	Organic carbon	8 960 ± 30	5 008	4 627
72–74	Organic carbon	16 400 ± 50	5 008	13 988
74–76	Organic carbon	17 520 ± 50	5 008	15 143
136–138	Organic carbon	25 610 ± 100	5 008	–
138–140	Organic carbon	24 910 ± 90	5 008	20 385
154–156	Organic carbon	26 390 ± 110	5 008	–
204–206	Organic carbon	25 040 ± 100	5 008	23 755
206–208	Organic carbon	27 410 ± 130	5 008	–
230–232	Organic carbon	25 420 ± 100	5 008	24 762

Note: The calendar age was obtained by subtracting the sum of the carbon reservoir age and the old carbon age (5 008 a) from the age fitted using the Bacon 2.3.3 program. − represents no data.

sults are primarily used for analyzing relative variation trends, revealing the relative changes of RSE across different layers or time series (Liu et al., 2015). The mean of the standardized data is 0; a *Z*-score greater than 0 indicates element enrichment, while a *Z*-score less than 0 suggests depletion, reflecting the evolution of different redox environments (Liu et al., 2015; Song et al., 2019). For example, a high *Z*-score for Mn typically indicates an oxidizing environment, whereas high *Z*-scores for U and Mo may suggest anoxic or reducing conditions (Tribovillard et al., 2006; Wang et al., 2019; Yang et al., 2021). *Z*-score normalization eliminates concentration differences among redox-sensitive elements, ensuring comparability in statistical analysis and aiding in environmental comparisons (Liu et al., 2015; Jolliffe, 2002). However, it can be sensitive to extreme values and mainly highlights relative rather than absolute changes, potentially masking important trends. To address this, the study combines original data trends and cross-validates with different elements to ensure the *Z*-score reflects true environmental changes, not artifacts from standardization. After *Z*-score standardization, the trends of multiple redox-sensitive indicators align with those of the original data. This indicates that although the standardization removed the magnitude differences between the concentrations of various elements, the change patterns in redox conditions reflected by the different elements have been accurately preserved. Specifically, the standardized trends are consistent with the fluctuations of redox conditions observed in the original data, without significant deviation. Therefore, it can be confirmed that *Z*-score standardization effectively retained the change characteristics of redox conditions across different stages and did not disproportionately affect the relative change trends of the original data. This further validates the feasibility and effectiveness of the standardization method in multivariate analysis.

After *Z*-score standardization, the U/Th ratio of the ANT32-RB16C core sediments ranges from –1.07 to 3.16, which is below the oxic-to-anoxic boundary of 0.75, indicating an oxic environment. The Ni/Co ratio varies from –1.66 to 2.92, which is significantly lower than the oxic-anoxic boundary, also indicating an oxic environment.

As shown in Fig. 3, the oxidative environment indicators (Mn/Ti and Co/Ti) and the reductive environment in-

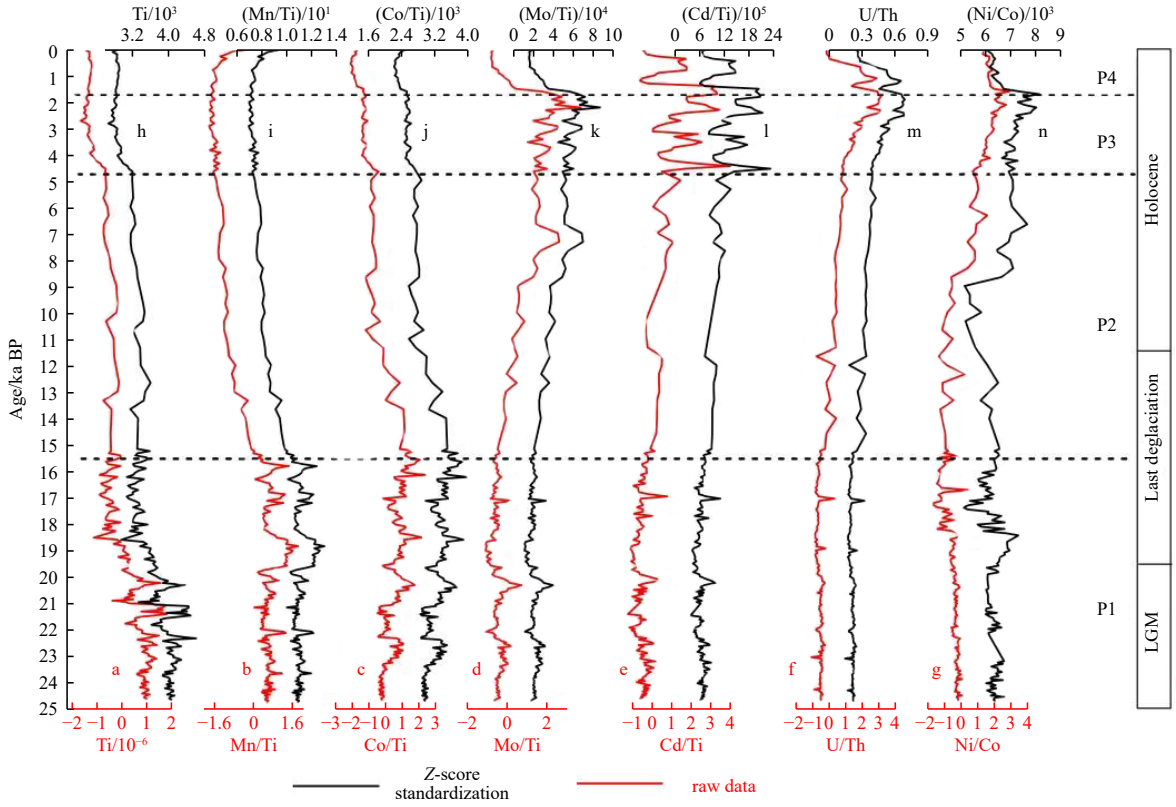


Fig. 3. Variations in oxidation intensity proxies in sediment core ANT32-RB16C. The Ti content in core ANT32-RB16C (*Z*-score standardization) (a), the Mn/Ti ratio in core ANT32-RB16C (*Z*-score standardization) (b), the Co/Ti ratio in core ANT32-RB16C (*Z*-score standardization) (c), the Mo/Ti ratio in core ANT32-RB16C (*Z*-score standardization) (d), the Cd/Ti ratio in core ANT32-RB16C (*Z*-score standardization) (e), the U/Th ratio in core ANT32-RB16C (*Z*-score standardization) (f), the Ni/Co ratio in core ANT32-RB16C (*Z*-score standardization) (g), the Ti content in core ANT32-RB16C (raw data) (h), the Mn/Ti ratio in core ANT32-RB16C (raw data) (i), the Co/Ti ratio in core ANT32-RB16C (raw data) (j), the Mo/Ti ratio in core ANT32-RB16C (raw data) (k), the Cd/Ti ratio in core ANT32-RB16C (raw data) (l), the U/Th ratio in core ANT32-RB16C (raw data) (m), the Ni/Co ratio in core ANT32-RB16C (raw data) (n).

dicators (Mo/Ti, Cd/Ti, U/Th, and Ni/Co) generally show a negative correlation. The changes can be divided into four phases.

(1) Phase 1 (24.7–15.7 cal ka BP)

During this phase, Mn/Ti fluctuates greatly but shows an overall increasing trend (Fig. 3b), with peaks at 16.9 cal ka BP, 18.8 cal ka BP, and 22.1 cal ka BP, reaching a maximum of 1.81. A trough appears at 21.2 cal ka BP with a value of 0.03, creating a fluctuation range of 1.78. Co/Ti, which represents oxidation and is related to the precipitation of iron-manganese oxides, shows a lag compared to Mn/Ti but follows a similar trend, with notable peaks at 16.2 cal ka BP, 18.2 cal ka BP, and 20.3 cal ka BP, with the highest value being 2.44 (Fig. 3c). In contrast, the reductive indicators (Mo/Ti, Cd/Ti, U/Th, and Ni/Co) remain low throughout this phase, with minimal fluctuations. Peaks occur around 17.1 cal ka BP to 16.8 cal ka BP, with values of 0.28, 0.76, 0.33, and 0.42, respectively, while troughs occur between 11.1 cal ka BP and 10.7 cal ka BP.

(2) Phase 2 (15.7–4.5 cal ka BP)

Both Mn/Ti and Co/Ti show a significant decline compared to Phase 1 (Figs 3b and c). Mn/Ti decreases from 0.75 at the beginning of Phase 2 to –1.59 by its end. Co/Ti also declines, though it fluctuates more frequently. The reductive indicators, Mo/Ti and Cd/Ti, increase, with Mo/Ti peaking sharply at 7.0 cal ka BP to 7.6 cal ka BP, and Cd/Ti showing larger fluctuations, especially at 11.0 cal ka BP, 7.6 cal ka BP, and 6.6 cal ka BP. U/Th and Ni/Co show a more gradual rise, with occasional peaks but without crossing the boundary into anoxic conditions (Figs 3f and g).

(3) Phase 3 (4.5–1.5 cal ka BP)

The oxidative indicators (Mn/Ti and Co/Ti) show a further decrease, with Mn/Ti ranging from –1.37 to –1.59 and Co/Ti from –0.84 to –1.72 (Figs 3b and c). On the other hand, the reductive indicators increase significantly compared to Phase 2, with Mo/Ti peaking at 3.7 cal ka BP, 3.0 cal ka BP, and 2.2 cal ka BP, reaching values as high as 3.72. Cd/Ti also shows a sharp increase, peaking at 3.50 at 2.4 cal ka BP.

(4) Phase 4 (1.5–0 cal ka BP)

Mn/Ti increases sharply, reaching values between –1.72 and –0.37, while Co/Ti declines early in this phase, reaching a trough at 0.5 cal ka BP before rising again (Fig. 3c). Reductive indicators show varied changes: Mo/Ti fluctuates between –0.60 and 0.24, and Cd/Ti drops rapidly from 3.23 to –0.63 after Phase 4 begins, with a subsequent increase (Figs 3d and e).

4.3 *Changes in grain size (>63 μm)*

The proportion of IRD varies from 8.01% to 41.18%, with an average of 20.32% (Fig. 4n). During 23.55–20.2 cal ka BP, the IRD content fluctuates frequently, reaching its highest variability during 23.0–20.2 cal ka BP. At 20.2–13.1 cal ka BP, IRD decreases overall, with some brief but sharp fluctuations. At 13.1–3.1 cal ka BP, the IRD content declines steadily, and at 3.1 cal ka BP, it rises again, reaching 16.2% by the end of the deposition process.

5 Discussion

5.1 *High oxidation environment stage (P1)*

This stage spans the LGM and the early period of the last deglaciation (24.7–15.6 cal ka BP), lasting approximately 9.1 ka. During this time, the oxidizing environment exhibits a pronounced peak. The oxidation indicator Mn/Ti indicates a significant accumulation of Mn, resulting in the formation of oxidized precipitates, with Co also adsorbing and depositing in large quantities. Both oxidation indicators reach high values, with multiple peaks observed (Fig. 4h). Conversely, reduction environment indicators such as Mo/Ti and U/Th show low values during this period; although peaks occasionally occur, the overall levels remain low, and the duration of these peaks is short, having little effect on trend changes (Figs 4j and k). Additionally, U/Th consistently stays below the critical threshold for the transition from oxic to suboxic conditions, indicating that the study area remains in an oxygen-rich environment.

As a decisive factor for redox environments, changes in oxygen levels are crucial, with deep ocean oxygen replenishment primarily dependent on ocean circulation (Stramma and Schmidtko, 2021; Tabata, 1961). Global thermohaline circulation transports oxygen-rich surface water into the deep ocean, influencing oxygen distribution in deeper water (Clark et al., 2002). In polar regions, cooling seawater sinks due to increased density, carrying large amounts of oxygen into the deep ocean and forming deep water (Orsi et al., 1999). This cooling effect is particularly pronounced in the Antarctic and Arctic regions. As these oxygen-rich waters circulate globally, they gradually transfer oxygen to deep marine environments, maintaining oxygen supply in the deep ocean (Johnson, 2008; Solodoch et al., 2022).

The retreat of sea ice is a critical factor for oxygen replenishment. Climate-induced melting in high-latitude regions exposes ocean surfaces, facilitating gas exchange between the atmosphere and the ocean. This process alters seawater density, enhancing vertical mixing and oxygen transport at various depths (Pedro et al., 2016; Nie et al., 2015). Furthermore, sea ice retreat increases photosynthetic efficiency by providing more open water areas, which improves atmospheric exchange and contributes to oxygen replenishment.

In the Ross Sea, a major site for the formation of RSBW (Budillon et al., 2011; Whitworth and Orsi, 2006), the process is especially significant. During the LGM, global temperatures remained low, even as they began to rise slowly in the early phase of the last deglaciation (19.6–15.6 cal ka BP), as seen in $\delta^{18}O$ data from Antarc-

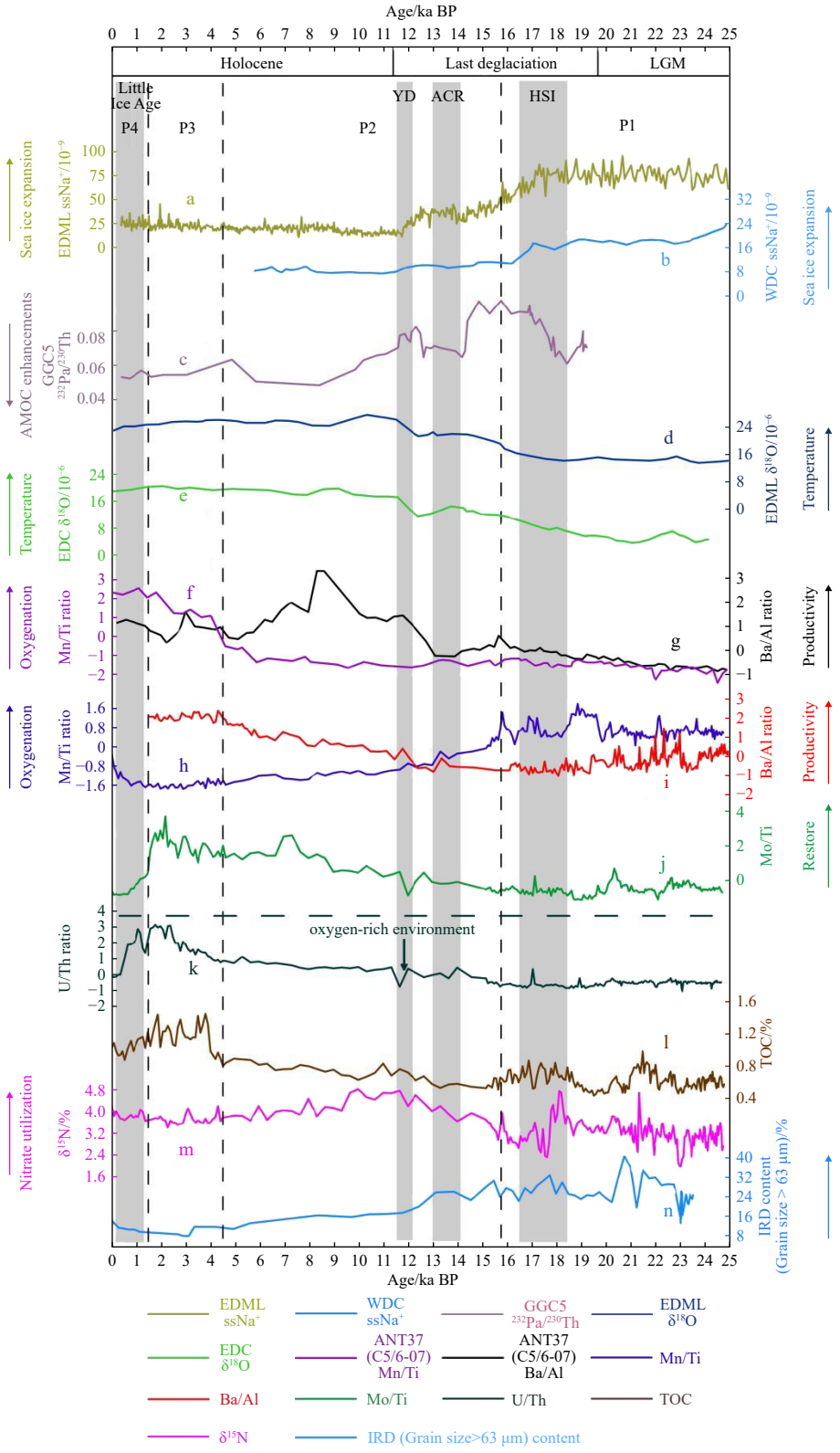


Fig. 4. The comprehensive comparison of redox changes in ANT32-RB16C, including various proxy indicators and other climatic environmental proxies. EDML $ssNa^+$ content (Fischer et al., 2007) (a), WDC $ssNa^+$ content (WAIS Divide Project Members, 2015) (b), GGC5 $^{232}Pa/^{230}Th$ (Hinkley and Matsumoto, 2001) (c), EDML $\delta^{18}O$ (Epica Community Members, 2006) (d), EDC $\delta^{18}O$ (Schmitt et al., 2012) (e), the Mn/Ti ratio in core ANT37-C5/6-07 (Hu et al., 2023) (f), the productivity in core ANT37-C5/6-07 (Hu et al., 2023) (g), the Mn/Ti ratio in core ANT32-RB16C (h), the productivity in core ANT32-RB16C (i), the Mo/Ti ratio in core ANT32-RB16C (j), the U/Th ratio in core ANT32-RB16C (k), the TOC proportion in core ANT32-RB16C (l), the $\delta^{15}N$ in core ANT32-RB16C (m), the >63 μm grain size fraction in core ANT32-RB16C (n).

tic ice cores (EDML and EDC) (Figs 4d and e). Cold air and strong winds in polar seas cool surface waters, increasing their density through sea ice formation and salinity. These denser waters sink, creating RSBW. This process transports oxygen-rich surface waters into the deep ocean, replenishing oxygen and sustaining deep water circulation, which ensures elevated oxygen concentrations in bottom waters over time. As a key component of global thermohaline circulation, RSBW is essential for the long-term maintenance of oxygen levels in deep-sea environments.

The first stage is generally characterized by a strong oxidizing environment, but with variations in oxidation levels. The peak occurs at the onset of the last deglaciation (19.6–18.5 cal ka BP) and lasts about 1.1 ka, showing significantly higher oxidation levels than other periods, despite no substantial climatic changes, as indicated by reduction indicators. Therefore, the peaks are considered normal, with lower levels in other periods influenced by other factors. Core data from the Indian Ocean sector (ANT37-C5/6-07) shows a reducing environment during this period, aligning with surface productivity changes and indicating a strong correlation between productivity and oxidation levels. During the LGM, productivity remained high but was still low overall, with higher nutrient levels and nitrate utilization compared to other stages. This elevated productivity contributed to oxygen consumption, causing lower oxidation levels despite a generally high-oxidation environment. The weakening of oxidation conditions during Heinrich Stadial 1 (HS1) (16.4–18.3 cal ka BP) differed from the LGM, possibly due to the intensification of AMOC, which weakened and caused heat accumulation in the Southern Ocean (Hinkley and Matsumoto, 2001; Shi, 2018), raising temperatures and increasing surface sea temperatures (Long et al., 2024). This enhanced water stratification, hindering mixing and affecting RSBW formation, led to a slight decrease during the peak oxidation conditions.

5.2 *Oxidation environment weakening stage (P2)*

The second stage (15.7–4.5 cal ka BP) begins around 15.7 cal ka BP, coinciding with the HS1 and the Antarctic cold reversal (ACR, 12.9–14.0 cal ka BP) interval, and continues until the late Holocene at 1.5 cal ka BP, lasting approximately 14.2 ka. Quantitative indicators show that the study area remains in an oxygen-rich condition but with significant changes. The Mn/Ti ratio begins to decline gradually, with some periods exhibiting brief peaks, but the overall trend remains unchanged. Similarly, U/Th and Mo/Ti ratios show troughs but display a clear upward trend, indicating a decline in the oxidation levels in the study area.

This phenomenon is linked to changes in oxygen levels. Increased surface productivity leads to substantial organic matter deposition, consuming oxygen and reducing water oxygen content, which deteriorates redox conditions (Anderson et al., 2009; Frank et al., 2000; Jaccard et al., 2013; Kohfeld et al., 2005). Temperature also plays a crucial role, as warmer temperatures decrease oxygen solubility in seawater, and reduced cold water formation or less deep-water descent prevents oxygen-rich water from reaching deep ocean areas, depleting oxygen and causing hypoxic or anoxic conditions (Adkins, 2013; Adkins et al., 2002; Bouttes et al., 2010; Ferrari et al., 2014; Gibson et al., 1999; Watson and Naveira, 2006; Wolff et al., 2010).

As temperatures rose (Figs 4e and f), ice-rafted debris significantly decreased, reflecting a rise in surface productivity. Total organic carbon (TOC) and biogenic barium (Bio Ba) showed significant changes, and $\delta^{15}N$ increased (Figs 4i, l and m), indicating more nitrate use and substantial organic matter deposition. This consumed oxygen, worsening redox conditions. While oxygen levels remained relatively high due to factors like RSBW, temperature rise limited ocean circulation, leading to ineffective oxygen replenishment in deep waters and a continuous decline in redox conditions (Mensah et al., 2021; Orsi et al., 1999; Chen et al., 2023; Sha et al., 2020).

Throughout this stage, significant climate changes occurred. Following HS1, Antarctic temperatures did not continue to rise but gradually declined, entering ACR. Despite the ongoing downward trend in oxidation conditions during the ACR, clear peaks appeared, indicating temporary improvements in the oxidation environment (Figs 4f, h, and j). During this time, the enhancement of oxidation conditions was influenced to some extent by a brief intensification of RSBW, which provided oxygen to the deep water. Additionally, the decrease in temperature and delayed retreat of sea ice (Figs 4a and b, d and e, and n) impacted productivity and dissolved oxygen levels. Furthermore, the strengthening of the AMOC was also a significant factor contributing to the improvement of the oxidation environment at this time.

At this time, ANT37-C5/6-07 shows an opposite trend, with its oxidation environment sharply increasing after the ACR. However, studies on the Ross Sea's redox conditions, like Cui et al. (2021), suggest that deep-water circulation worsened and bottom-waters upwelling weakened, indicating a relatively weak oxidation environment. Wang et al. (2018) also found four oxidation pulses in the Ross Sea, possibly linked to enhanced circulation, highlighting the differing redox conditions between the Astronaut Sea and the Ross Sea, despite similar productivity changes during the ACR.

During the ACR, although productivity increased in both areas, the redox trends were different due to sea ice cover and water mass movement. In the Ross Sea, strong sea ice and weakened bottom waters upwelling led to insufficient oxygen supply, causing a decline in redox conditions. In contrast, the Astronaut Sea experienced sea ice retreat, warming surface waters, and enhanced bottom waters upwelling, which improved oxygen replenishment and enhanced the oxidation environment. Thus, despite in-

creased productivity, the differences in bottom waters upwelling, sea ice, and water mass movement resulted in a weakening of oxidation in the Ross Sea and an enhancement in the Astronaut Sea.

The Younger Dryas (YD, 11.7–12.2 cal ka BP) represents a sudden cooling event during the warming process of the last deglaciation, with temperatures rapidly dropping to levels near the last glacial period. However, the Antarctic did not experience a similar degree of cooling and remained in a relatively warm state, a phenomenon associated with the "seesaw" mechanism of climate between the Northern and Southern Hemispheres (Landais et al., 2015). During this period, the redox environment in the study area underwent significant changes. While oxidative indicators showed a slight decrease, the decline was not substantial, whereas reductive indicators increased notably. This shift can be attributed to several interconnected environmental mechanisms. First, rising temperatures intensified water stratification, limiting deep water oxygenation and promoting reductive element accumulation. Second, the retreat of sea ice reduced nutrient availability, suppressed primary productivity, and lowered oxygen consumption, reflected by a drop in $\delta^{15}N$. Lastly, increased temperatures likely accelerated organic matter decomposition, further depleting oxygen in deep waters. In summary, the YD redox changes were driven by sea ice retreat, temperature rise, and intensified stratification, leading to a shift toward more reductive conditions.

The study area experienced a brief improvement in oxidation conditions during the ACR period, followed by a gradual decline in temperatures. The overall warming trend in the study area led to a reduction in the extent of sea ice in the Antarctic, weakening the cooling effect and the formation of RSBW, thereby reducing the oxygen supply to deep waters. Additionally, the retreat of sea ice contributed to an increase in primary productivity (Figs 4i, l, and m), resulting in higher organic carbon deposition and decomposition, consuming more oxygen. The combination of insufficient oxygen supply in deep waters, increased productivity, and enhanced organic matter decomposition led to a decline in the oxidation environment. The oxidation environment in the Astronaut Sea remained at high levels throughout the P2 stage due to the influence of sea ice coverage and water mass factors, reaching a peak between 8.5 cal ka BP and 9.0 cal ka BP.

5.3 *Oxidation environment stable fluctuation stage (P3)*

The third stage (4.5–1.5 cal ka BP) represents a relatively unique phase in the sedimentary record. During this period, although oxidation indicators exhibited a declining trend, the changes were minor and remained within a narrow range of fluctuations, suggesting a continued weakening of oxidative conditions. In contrast, reduction indicators showed pronounced responses. The U/Th ratio indicated that, while conditions remained oxygen-rich, elemental levels approached the threshold for oxygen-rich environments. Notably, the two reduction indicators increased significantly and displayed wide fluctuations, contrasting sharply with the relatively stable oxidation indicators (Figs 4h, j and k). This pattern suggests that the study area was transitioning into a phase of enhanced reducing conditions.

This phenomenon reflects substantial oxygen consumption, likely driven by several factors, including increased productivity, organic matter deposition, and reduced ocean circulation. Productivity levels underwent significant changes during this stage, reaching extremely high values compared to the previous two phases (Figs 4i and l). Other climatic factors remained relatively stable, implying that productivity changes may have played a dominant role. The high productivity led to substantial organic matter deposition, with its subsequent degradation consuming oxygen and intensifying reducing reactions. The influx of organic matter likely stimulated the activity of anaerobic microorganisms in bottom waters or sediments, releasing more reducing substances such as hydrogen sulfide. Meanwhile, oxidative reactions did not intensify significantly due to insufficient oxygen availability.

5.4 *Rapid recovery stage of the oxidation environment (P4)*

The fourth stage (1.5–0 cal ka BP) occurs at the end of the Holocene. At this time, the Mn/Ti and Co/Ti ratios suddenly increased, but the increase was slow. The Mo/Ti ratio, which represents the reductive environment, continued to decline, while the Cd/Ti ratio, which also indicates the reductive environment, showed a sharp increase around 1.2–0.5 cal ka BP (Figs 4h, j, and k), although its overall trend is similar to Mo/Ti. It is speculated that this may be related to the different affinities of Cd and Mo for sulfur. Cd has a closer affinity to sulfur, and the formation of cadmium sulfide deposits may lead to an increase in the Cd/Ti ratio. In contrast, Mo has a weaker affinity for sulfur. Therefore, the sudden increase and decrease in the Cd/Ti ratio may be related to changes in sulfur deposition, especially in cases where the oxidative environment is undergoing complex changes. The combination and release of cadmium and sulfur directly affect its concentration. The U/Th values indicate that the oxidation environment of the water body increased from near hypoxic levels in the third stage to a high-oxygen environment, even reaching the highest level observed throughout the sedimentary process, suggesting a rapid enhancement of the oxidation environment.

After enduring stable climatic changes during the Holocene, the Little Ice Age (LIA, 1.5–0 cal ka BP) suddenly emerged, with cooling temperatures and expanded sea ice enhancing the oxidation environment in the Ross Sea (Kajanto et al., 2024; Matthews and Briffa, 2005). This process also facilitated a brief intensification of RS-

BW, providing oxygen to deep waters. Meanwhile, the continuously declining levels of productivity limited organic matter deposition, consequently reducing oxygen consumption.

6 Conclusions

This study reveals significant changes in the redox environment of the study area since the LGM, demonstrating the profound impact of global climate change on deep-sea oxygen supply and organic matter degradation processes. Through detailed tracking of redox condition changes, the study shows that rising temperatures, ice shelf retreat, and increased productivity have strengthened reducing conditions, while the glacial period accelerated the formation of oxidation environments. Notably, peak oxidation conditions occurred during the LGM and the early deglaciation phase (24.7–15.6 cal ka BP), maintained primarily by deep water circulation and the formation and transport of RSBW. Subsequently, during the late deglaciation and early Holocene (15.7–4.5 cal ka BP), oxidation conditions gradually declined, with sea ice retreat and increased productivity leading to organic matter deposition and oxygen consumption in deep waters. In the late Holocene (4.5–1.5 cal ka BP), the redox environment continued to weaken, indicating the dominant role of productivity changes in this phase. Finally, during the LIA, the redox environment rapidly recovered, closely linked to climate cooling, sea ice expansion, and the strengthening of RSBW. This study demonstrates how global climate change, sea ice dynamics, and productivity fluctuations collectively impact deep-sea oxygen supply and redox environments. It also highlights the close relationship between changes in redox conditions, climate, vertical ocean mixing, and biological productivity. By providing a new perspective, this work deepens the understanding of the interaction between climate change and deep-sea oxygen circulation, offering valuable data support for future polar ocean system research.

Acknowlegements

We are very grateful to all of the scientific expedition staff, especially the teachers and students of the Marine Geology and the Geophysics Working Group, and all of the crew of the R/V *Xuelong* icebreaker for their hard work in sampling during the 32th Chinese Antarctic Research Expedition. We sincerely thank the Chinese Arctic and Antarctic Administration and Polar Research Institute of China for their great help in this research.

References

Adelson J M, Helz G R, Miller C V. 2001. Reconstructing the rise of recent coastal anoxia; molybdenum in Chesapeake Bay sediments. Geochimica et Cosmochimica Acta, 65(2): 237–252, doi: 10.1016/S0016-7037(00)00539-1

Adkins J F. 2013. The role of deep ocean circulation in setting glacial climates. Paleoceanography, 28(3): 539–561, doi: 10.1002/palo.20046

Adkins J F, McIntyre K, Schrag D P. 2002. The salinity, temperature, and $\delta^{18}O$ of the glacial deep ocean. Science, 298(5599): 1769–1773, doi: 10.1126/science.1076252

Algeo T J, Hinnov L, Moser J, et al. 2010. Changes in productivity and redox conditions in the Panthalassic Ocean during the latest Permian. Geology, 38(2): 187–190, doi: 10.1130/G30483.1

Algeo T J, Liu Jiangsi. 2020. A re-assessment of elemental proxies for paleoredox analysis. Chemical Geology, 540: 119549, doi: 10.1016/j.chemgeo.2020.119549

Algeo T J, Maynard J B. 2004. Trace-element behavior and redox facies in core shales of Upper Pennsylvanian Kansas-type cyclothems. Chemical Geology, 206(3–4): 289–318, doi: 10.1016/j.chemgeo.2003.12.009

Anderson J B, Conway H, Bart P J, et al. 2014. Ross Sea paleo-ice sheet drainage and deglacial history during and since the LGM. Quaternary Science Reviews, 100: 31–54, doi: 10.1016/j.quascirev.2013.08.020

Anderson J B, Shipp S S, Lowe A L, et al. 2002. The Antarctic Ice Sheet during the Last Glacial Maximum and its subsequent retreat history: a review. Quaternary Science Reviews, 21(1–3): 49–70, doi: 10.1016/S0277-3791(01)00083-X

Anderson R F, Ali S, Bradtmiller L I, et al. 2009. Wind-driven upwelling in the Southern Ocean and the deglacial rise in atmospheric CO_2. Science, 323(5920): 1443–1448, doi: 10.1126/science.1167441

Baloza M, Henkel S, Geibert W, et al. 2022. Benthic carbon remineralization and iron cycling in relation to sea ice cover along the eastern continental shelf of the Antarctic Peninsula. Journal of Geophysical Research: Oceans, 127(7): e2021JC018401, doi: 10.1029/2021JC018401

Baloza M, Henkel S, Kasten S, et al. 2023. The impact of sea ice cover on microbial communities in Antarctic shelf sediments. Microorganisms, 11(6): 1572, doi: 10.3390/microorganisms11061572

Basak C, Pahnke K, Frank M, et al. 2015. Neodymium isotopic characterization of Ross Sea Bottom Water and its advection through the southern South Pacific. Earth and Planetary Science Letters, 419: 211–221, doi: 10.1016/j.epsl.2015.03.011

Bouttes N, Paillard D, Roche D M. 2010. Impact of brine-induced stratification on the glacial carbon cycle. Climate of the Past, 6(5): 575–589, doi: 10.5194/cp-6-575-2010

Brown E T, Le Callonnec L, German C R. 2000. Geochemical cycling of redox-sensitive metals in sediments from Lake Malawi: a diagnostic paleotracer for episodic changes in mixing depth. Geochimica et Cosmochimica Acta, 64(20): 3515–3523, doi: 10.1016/S0016-7037(00)00460-9

Budillon G, Castagno P, Aliani S, et al. 2011. Thermohaline variability and Antarctic bottom water formation at the Ross Sea shelf break. Deep-Sea Research Part Ⅰ:

Oceanographic Research Papers, 58(10): 1002–1018, doi: 10.1016/j.dsr.2011.07.002

Calvert S E, Pedersen T F. 1993. Geochemistry of recent oxic and anoxic marine sediments: implications for the geological record. Marine Geology, 113(1–2): 67–88, doi: 10.1016/0025-3227(93)90150-T

Calvert S E, Pedersen T F. 1996. Sedimentary geochemistry of manganese; implications for the environment of formation of manganiferous black shales. Economic Geology, 91(1): 36–47, doi: 10.2113/gsecongeo.91.1.36

Carmack E C, Killworth P D. 1978. Formation and interleaving of abyssal water masses off Wilkes Land, Antarctica. Deep-Sea Research, 25(4): 357–369, doi: 10.1016/0146-6291(78)90563-5

Chang Huajin, Zhu Xuelei, Feng Lianjun, et al. 2009. Redox sensitive trace elements as paleoenvironments proxies. Geological Review (in Chinese), 55(1): 91–99

Chen Yangjun, Chen Jinxu, Wang Yi, et al. 2023. Sources and transformations of nitrite in the Amundsen Sea in summer 2019 and 2020 as revealed by nitrogen and oxygen isotopes. Acta Oceanologica Sinica, 42(4): 16–24, doi: 10.1007/s13131-022-2111-4

Clark P U, Pisias N G, Stocker T F, et al. 2002. The role of the thermohaline circulation in abrupt climate change. Nature, 415(6874): 863–869, doi: 10.1038/415863a

Colman A S, Holland H D. 2000. The global diagenetic flux of phosphorus from marine sediments to the oceans: Redox sensitivity and the control of atmospheric oxygen levels. In: Glenn C R, Prévôt-Lucas L, Lucas J, eds. Marine Authigenesis: From Global to Microbial. SEPM Society for Sedimentary Geology, 53–75

Cui Chao, Tang Zheng, Rebesco M, et al. 2021. Sedimentary records of enhanced deep ventilation during the last deglacialtion in the Ross Sea, Southern Ocean. Quaternary Sciences (in Chinese), 41(3): 678–690

Diekmann B, Kuhn G. 1999. Provenance and dispersal of glacial–marine surface sediments in the Weddell Sea and adjoining areas, Antarctica: ice-rafting versus current transport. Marine Geology, 158(1–4): 209–231, doi: 10.1016/S0025-3227(98)00165-0

Dinniman M S, Klinck J M, Smith W O Jr. 2011. A model study of Circumpolar Deep Water on the West Antarctic Peninsula and Ross Sea continental shelves. Deep-Sea Research Part Ⅱ: Topical Studies in Oceanography, 58(13–16): 1508–1523, doi: 10.1016/j.dsr2.2010.11.013

EPICA Community Members. 2006. One-to-one coupling of glacial climate variability in Greenland and Antarctica. Nature, 444(7116): 195–198, doi: 10.1038/nature05301

Fan Qi, Fan Tailiang, Li Yifan, et al. 2020. Paleo-environments and development pattern of high-quality marine source rocks of the Early Cambrian, Northern Tarim Platform. Earth Science (in Chinese), 45(1): 285–302

Fan Qiushuang, Xia Guoqing, Li Gaojie, et al. 2022. Analytical methods and research progress of redox conditions in the paleo-ocean. Acta Sedimentologica Sinica (in Chinese), 40(5): 1151–1171

Ferrari R, Jansen M F, Adkins J F, et al. 2014. Antarctic sea ice control on ocean circulation in present and glacial climates. Proceedings of the National Academy of Sciences of the United States of America, 111(24): 8753–8758, doi: 10.1073/pnas.1323922111

Fischer H, Fundel F, Ruth U, et al. 2007. Reconstruction of millennial changes in dust emission, transport and regional sea ice coverage using the deep EPICA ice cores from the Atlantic and Indian Ocean sector of Antarctica. Earth and Planetary Science Letters, 260(1–2): 340–354, doi: 10.1016/j.epsl.2007.06.014

Frank M, Gersonde R, Van Der Loeff M R, et al. 2000. Similar glacial and interglacial export bioproductivity in the Atlantic Sector of the Southern Ocean: Multiproxy evidence and implications for glacial atmospheric CO_2. Paleoceanography, 15(6): 642–658, doi: 10.1029/2000PA000497

Gersonde R, Crosta X, Abelmann A, et al. 2005. Sea-surface temperature and sea ice distribution of the Southern Ocean at the EPILOG Last Glacial Maximum—a circum-Antarctic view based on siliceous microfossil records. Quaternary Science Reviews, 24(7–9): 869–896, doi: 10.1016/j.quascirev.2004.07.015

Gibson J A E, Trull T, Nichols P D, et al. 1999. Sedimentation of ^{13}C-rich organic matter from Antarctic sea-ice algae: A potential indicator of past sea-ice extent. Geology, 27(4): 331–334, doi: 10.1130/0091-7613(1999)027<0331:SOCROM>2.3.CO;2

Guo Guijun, Shi Jiuxin, Jiao Yutian. 2016. Turbulent mixing in the upper ocean of the northwestern Weddell Sea, Antarctica. Acta Oceanologica Sinica, 35(3): 1–9, doi: 10.1007/s13131-016-0816-y

Hinkley T K, Matsumoto A. 2001. Atmospheric regime of dust and salt through 75, 000 years of Taylor Dome ice core: refinement by measurement of major, minor, and trace metal suites. Journal of Geophysical Research: Atmospheres, 106(D16): 18487–18493, doi: 10.1029/2000JD900550

Hu Liangming, Zhang Yi, Wang Yizhuo, et al. 2023. Paleoproductivity and deep-sea oxygenation in Cosmonaut Sea since the last glacial maximum: impact on atmospheric CO_2. Frontiers in Marine Science, 10: 1215048, doi: 10.3389/fmars.2023.1215048

Huang Yongjian, Wang Chengshan, Wang Yunliang. 2005. Progress in the study of proxies of paleocean productivity. Earth Science Frontiers (in Chinese), 12(2): 163–170

Huang Mengxue, Wang Rujian, Xiao Wenshen, et al. 2016. Retreat process of Ross Ice Shelf and hydrodynamic changes on northwestern Ross continental shelf since the last glacial. Marine Geology & Quaternary Geology (in Chinese), 36(5): 97–108

Huang Shaojian, Wang Feiyue, Yuan Tengfei, et al. 2023. Modeling the mercury cycle in the sea ice environment: a buffer between the polar atmosphere and ocean. Environmental Science & Technology, 57(39): 14589–14601

Jaccard S L, Hayes C T, Martínez-García A, et al. 2013. Two modes of change in southern ocean productivity over the

past million years. Science, 339(6126): 1419–1423, doi: 10.1126/science.1227545

Jacobs S S, Amos A F, Bruchhausen P M. 1970. Ross sea oceanography and Antarctic bottom water formation. Deep-Sea Research and Oceanographic Abstracts, 17(6): 935–962, doi: 10.1016/0011-7471(70)90046-X

Johnson G C. 2008. Quantifying Antarctic bottom water and North Atlantic deep water volumes. Journal of Geophysical Research: Oceans, 113(C5): C05027

Jolliffe I T. 2002. Principal component analysis for special types of data. In: Principal Component Analysis. 2nd ed. New York: Springer, 338–372

Kajanto K, Andresen C, Seroussi H, et al. 2024. Holocene warmth explains the Little Ice Age advance of Sermeq Kujalleq. Quaternary Science Reviews, 341: 108840, doi: 10.1016/j.quascirev.2024.108840

Kohfeld K E, Quéré C L, Harrison S P, et al. 2005. Role of marine biology in glacial-interglacial CO_2 cycles. Science, 308(5718): 74–78, doi: 10.1126/science.1105375

Landais A, Masson-Delmotte V, Stenni B, et al. 2015. A review of the bipolar see-saw from synchronized and high resolution ice core water stable isotope records from Greenland and East Antarctica. Quaternary Science Reviews, 114: 18–32, doi: 10.1016/j.quascirev.2015.01.031

Lei Ziyan, Ge Qian, Chen Dong, et al. 2022. Provenance of sediments in the Amundsen Sea, West Antarctic since the mid-Holocene and paleoclimate reconstruction. Earth Science Frontiers (in Chinese), 29(4): 179–190, doi: 10.13745/j.esf.sf.2022.1.7

Lenton T M. 2000. Land and ocean carbon cycle feedback effects on global warming in a simple Earth system model. Tellus B, 52(5): 1159–1188, doi: 10.3402/tellusb.v52i5.17097

Li Yifan, Fan Tailiang, Zhang Jinchuan, et al. 2015. Impact of paleoenvironment, organic paleoproductivity, and clastic dilution on the formation of organic-rich shales: a case study about the Ordovician-Silurian black shales, southeastern Chongqing, South China. Arabian Journal of Geosciences, 8(12): 10225–10239, doi: 10.1007/s12517-015-1944-y

Licht K J, Dunbar N W, Andrews J T, et al. 1999. Distinguishing subglacial till and glacial marine diamictons in the western Ross Sea, Antarctica: implications for a last glacial maximum grounding line. GSA Bulletin, 111(1): 91–103, doi: 10.1130/0016-7606(1999)111<0091:DSTAGM>2.3.CO;2

Liu Helin, Chen Zhihua, Ge Shulan, et al. 2015. Late Quaternary sedimentary records and paleoceanographic implications from the core on continental slope off the Prydz Bay, East Antarctic. Marine Geology & Quaternary Geology (in Chinese), 35(3): 209–217, doi: 10.3724/SP.J.1140.2015.03209

Liu Shuaibin, Zhou Chunxia, Wang Zemin. 2016. Comparative analysis of changes in sea ice extent in Ross Sea and Prydz Bay. Chinese Journal of Polar Research (in Chinese), 28(2): 228–234

Long Feijiang, Xiang Bo, Wang Yizhuo, et al. 2024. Evolution of paleoproductivity in the Antarctica Ross Sea since the Last Glacial Maximum. Marine Geology and Quaternary Geology (in Chinese), 44(1): 109–120

Mansour A, Wagreich M, Gentzis T, et al. 2020. Depositional and organic carbon-controlled regimes during the Coniacian-Santonian event: First results from the southern Tethys (Egypt). Marine and Petroleum Geology, 115: 104285, doi: 10.1016/j.marpetgeo.2020.104285

Matthews J A, Briffa K R. 2005. The 'Little Ice Age': Re-evaluation of an Evolving Concept. Geografiska Annaler: Series A, Physical Geography, 87(1): 17–36

Mensah V, Nakayama Y, Fujii M, et al. 2021. Dense water downslope flow and AABW production in a numerical model: Sensitivity to horizontal and vertical resolution in the region off Cape Darnley polynya. Ocean Modelling, 165: 101843, doi: 10.1016/j.ocemod.2021.101843

Meyer K M, Ridgwell A, Payne J L. 2016. The influence of the biological pump on ocean chemistry: implications for long-term trends in marine redox chemistry, the global carbon cycle, and marine animal ecosystems. Geobiology, 14(3): 207–219, doi: 10.1111/gbi.12176

Monnin E, Steig E J, Siegenthaler U, et al. 2004. Evidence for substantial accumulation rate variability in Antarctica during the Holocene, through synchronization of CO_2 in the Taylor Dome, Dome C and DML ice cores. Earth and Planetary Science Letters, 224(1–2): 45–54, doi: 10.1016/j.epsl.2004.05.007

Morford J L, Emerson S. 1999. The geochemistry of redox sensitive trace metals in sediments. Geochimica et Cosmochimica Acta, 63(11–12): 1735–1750, doi: 10.1016/S0016-7037(99)00126-X

Mosola A B, Anderson J B. 2006. Expansion and rapid retreat of the West Antarctic Ice Sheet in eastern Ross Sea: possible consequence of over-extended ice streams?. Quaternary Science Reviews, 25(17–18): 2177–2196, doi: 10.1016/j.quascirev.2005.12.013

Muratli J M, Chase Z, McManus J, et al. 2010. Ice-sheet control of continental erosion in central and southern Chile (36°–41°S) over the last 30, 000 years. Quaternary Science Reviews, 29(23–24): 3230–3239, doi: 10.1016/j.quascirev.2010.06.037

Nie Senyan, Xiao Wenshen, Wang Rujian 2015. Palaeoclimatic changes of the Bransfield Strait, Antarctic Peninsula since 6 kaBP, and the tele-connection with ENSO. Marine Geology and Quaternary Geology (in Chinese), 35(3): 157–166

Olund S, Lyons W B, Welch S A, et al. 2018. Fe and nutrients in coastal Antarctic streams: Implications for primary production in the Ross Sea. Journal of Geophysical Research: Biogeosciences, 123(12): 3507–3522, doi: 10.1029/2017JG004352

Ordoñez Rendón L G, Neugebauer I, Thomas C, et al. 2024. Sediment-redox dynamics in an oligotrophic deep-water lake in Tierra del Fuego: insights from Fe isotopes. Journal of Paleolimnology, 72(2): 129–143, doi: 10.1007/s10933-024-00316-0

Orsi A H, Johnson G C, Bullister J L. 1999. Circulation, mixing, and production of Antarctic Bottom Water. Progress in Oceanography, 43(1): 55–109, doi: 10.1016/S0079-6611(99)00004-X

Orsi A H, Wiederwohl C L. 2009. A recount of Ross Sea waters. Deep-Sea Research Part Ⅱ: Topical Studies in Oceanography, 56(13–14): 778–795, doi: 10.1016/j.dsr2.2008.10.033

Ozaki K, Tajika E. 2013. Biogeochemical effects of atmospheric oxygen concentration, phosphorus weathering, and sea-level stand on oceanic redox chemistry: Implications for greenhouse climates. Earth and Planetary Science Letters, 373: 129–139, doi: 10.1016/j.epsl.2013.04.029

Pease C H. 1987. The size of wind-driven coastal polynyas. Journal of Geophysical Research: Oceans, 92(C7): 7049–7059, doi: 10.1029/JC092iC07p07049

Pedro J B, Bostock H C, Bitz C M, et al. 2016. The spatial extent and dynamics of the Antarctic Cold Reversal. Nature Geoscience, 9(1): 51–55, doi: 10.1038/ngeo2580

Rabalais N N, Turner R E, Scavia D. 2002. Beyond Science into Policy: Gulf of Mexico Hypoxia and the Mississippi River: Nutrient policy development for the Mississippi River watershed reflects the accumulated scientific evidence that the increase in nitrogen loading is the primary factor in the worsening of hypoxia in the northern Gulf of Mexico. BioScience, 52(2): 129–142, doi: 10.1641/0006-3568(2002)052[0129:BSIPGO]2.0.CO;2

Rintoul S R. 1985. On the origin and influence of Adélie Land Bottom Water. In: Jacobs S S, Weiss R F, eds. Ocean, Ice, and Atmosphere: Interactions at the Antarctic Continental Margin. American Geophysical Union, 75: 151–171

Russell A D, Morford J L. 2001. The behavior of redox-sensitive metals across a laminated–massive–laminated transition in Saanich Inlet, British Columbia. Marine Geology, 174(1–4): 341–354, doi: 10.1016/S0025-3227(00)00159-6

Schmitt J, Schneider R, Elsig J, et al. 2012. Carbon isotope constraints on the deglacial CO_2 rise from ice cores. Science, 336(6082): 711–714, doi: 10.1126/science.1217161

Sha Longbin, Li Dongling, Liu Yanguang, et al. 2020. Biogenic silica concentration as a marine primary productivity proxy in the Holsteinsborg Dyb, West Greenland, during the last millennium. Acta Oceanologica Sinica, 39(9): 78–85, doi: 10.1007/s13131-020-1648-3

Shi Jiuxin. 2018. A review of ice shelf-ocean interaction in Antarctica. Chinese Journal of Polar Research (in Chinese), 30(3): 287–302

Smith W O Jr, Ainley D G, Arrigo K R, et al. 2014. The oceanography and ecology of the Ross Sea. Annual Review of Marine Science, 6: 469–487, doi: 10.1146/annurev-marine-010213-135114

Smith W O Jr, Sedwick P N, Arrigo K R, et al. 2012. The Ross Sea in a sea of change. Oceanography, 25(3): 90–103, doi: 10.5670/oceanog.2012.80

Solodoch A, Stewart A L, Hogg A M, et al. 2022. How does Antarctic bottom water cross the Southern Ocean. Geophysical Research Letters, 49(7): e2021GL097211, doi: 10.1029/2021GL097211

Song Lehui, Han Xibin, Li Jiabiao, et al. 2019. Western Ross Sea sedimentary environment reconstruction since the Last Glacial Maximum based on organic carbon and biomarker analyses. Haiyang Xuebao (in Chinese), 41(9): 52–64

Stammerjohn S, Massom R, Rind D, et al. 2012. Regions of rapid sea ice change: An inter-hemispheric seasonal comparison. Geophysical Research Letters, 39(6): L06501

Stramma L, Schmidtko S. 2021. Spatial and temporal variability of oceanic oxygen changes and underlying trends. Atmosphere-Ocean, 59(2): 122–132, doi: 10.1080/07055900.2021.1905601

Tabata S. 1961. Temporal changes of salinity, temperature, and dissolved oxygen content of the water at Station "P" in the northeast Pacific Ocean, and some of their determining factors. Journal of the Fisheries Research Board of Canada, 18(6): 1073–1124, doi: 10.1139/f61-066

Tamura T, Ohshima K I, Nihashi S. 2008. Mapping of sea ice production for Antarctic coastal polynyas. Geophysical Research Letters, 35(7): L07606

Tribovillard N, Algeo T J, Lyons T, et al. 2006. Trace metals as paleoredox and paleoproductivity proxies: an update. Chemical Geology, 232(1–2): 12–32, doi: 10.1016/j.chemgeo.2006.02.012

WAIS Divide Project Members. 2015. Precise interpolar phasing of abrupt climate change during the last ice age. Nature, 520(7549): 661–665, doi: 10.1038/nature14401

Wang Jiakai, Li Tiegang, Xiong Zhifang, et al. 2018. Sedimentary gochemical characteristics of the Redox-sensitive elements in Ross Sea, Antarctica: Implications for paleoceanography. Marine Geology and Quaternary Geology (in Chinese), 38(5): 112–121

Wang Xiaojing, Li Li, Liu Jihua, et al. 2019. Early diagenesis of redox-sensitive trace metals in the northern Okinawa Trough. Acta Oceanologica Sinica, 38(12): 14–25, doi: 10.1007/s13131-019-1512-5

Watson A J, Garabato A C N. 2006. The role of Southern Ocean mixing and upwelling in glacial-interglacial atmospheric CO_2 change. Tellus B, 58(1): 73–87, doi: 10.1111/j.1600-0889.2005.00167.x

Wei Hengye. 2012. Productivity and redox proxies of palaeooceans: An overview of elementary geochemistry. Sedimentary Geology and Tethyan Geology (in Chinese), 32(2): 76–88

Whitworth T III, Orsi A H. 2006. Antarctic Bottom Water production and export by tides in the Ross Sea. Geophysical Research Letters, 33(12): L12609

Wignall P B, Twitchett R J. 1996. Oceanic anoxia and the end Permian mass extinction. Science, 272(5265): 1155–1158, doi: 10.1126/science.272.5265.1155

Wolff E W, Barbante C, Becagli S, et al. 2010. Changes in environment over the last 800, 000 years from chemical analysis of the EPICA Dome C ice core. Quaternary Science Reviews, 29(1–2): 285–295, doi: 10.1016/j.quascirev.2009.06.013

Xiu Chun, Du Ming, Zhang Xu, et al. 2020. Changes of marine productivity and sedimentary environment recorded by biogenic components in the Antarctica Ross Sea since the last deglaciation. Journal of Oceanology and Limnology, 38(6): 1746–1754, doi: 10.1007/s00343-019-9218-2

Xu Shumei, Zhang Xiaodong, Zhai Shikui, et al. 2007. The geochemistry of redox sensitive trace elements and their environmental implications. Marine Geology Letters (in Chinese), 23(3): 11–18

Yang Yamin, Zeng Zhigang, Yin Xuebo, et al. 2021. Mineralogy, geochemistry, and sulfur isotope characteristics of sediment-hosted hydrothermal sulfide minerals from the southern Okinawa Trough. Acta Oceanologica Sinica, 40(10): 129–143, doi: 10.1007/s13131-021-1836-9

Yokoyama Y, Anderson J B, Yamane M, et al. 2016. Widespread collapse of the Ross Ice Shelf during the late Holocene. Proceedings of the National Academy of Sciences of the United States of America, 113(9): 2354–2359

Zhang Run, Ma Qiang, Chen Min, et al. 2019. Nitrogen uptake regime regulated by ice melting during austral summer in the Prydz Bay, Antarctica. Acta Oceanologica Sinica, 38(8): 1–7, doi: 10.1007/s13131-019-1434-2